Enhanced Seebeck coefficient of quantum-confined electrons in $SrTiO_3/SrTi_{0.8}Nb_{0.2}O_3$ superlattices

Yoriko Mune
Graduate School of Engineering, Nagoya University, Furo-cho, Chikusa, Nagoya 464-8603, Japan

Hiromichi Ohta[a] and Kunihito Koumoto
Graduate School of Engineering, Nagoya University, Furo-cho, Chikusa, Nagoya 464-8603, Japan and CREST, Japan Science and Technology Agency, 4-1-8 Honcho, Kawaguchi 332-0012, Japan

Teruyasu Mizoguchi and Yuichi Ikuhara
Institute of Engineering Innovation, The University of Tokyo, 2-11-16 Yayoi, Bunkyo, Tokyo 113-8656, Japan

(Received 20 August 2007; accepted 21 October 2007; published online 8 November 2007)

We report two-dimensional Seebeck coefficients ($|S|_{2D}$) of $[(SrTiO_3)_x/(SrTi_{0.8}Nb_{0.2}O_3)_y]_{20}$ ($x=1-60$, $y=1-20$) superlattices, which were grown on the (100) face of insulating $LaAlO_3$ substrates to clarify the origin of the giant $|S|_{2D}$ values of the $SrTiO_3$ superlattices [H. Ohta *et al.*, Nat. Mater. **6**, 129 (2007)]. The $|S|_{2D}$ values of the $[(SrTiO_3)_{17}/(SrTi_{0.8}Nb_{0.2}O_3)_y]_{20}$ superlattices increased proportionally to $y^{-0.5}$ and reached 320 $\mu V\ K^{-1}$ ($y=1$), which is approximately five times larger than that of the $SrTi_{0.8}Nb_{0.2}O_3$ bulk ($|S|_{3D}=61\ \mu V\ K^{-1}$). The slope of the $\log|S|_{2D}$-$\log y$ plots was −0.5, proving that the density of states in the ground state for $SrTiO_3$ increases inversely proportionally to y. The critical barrier thickness for quantum electron confinement was also clarified to be 6.25 nm (16 unit cells of $SrTiO_3$). © *2007 American Institute of Physics*.
[DOI: 10.1063/1.2809364]

Two-dimensionally confined electrons in extremely narrow quantum wells (thickness ≤10 nm), the latter being composed of an electron pocket and a barrier, exhibit exotic electron transport properties as compared to the corresponding bulk materials due to the fact that the density of states (DOS) near the bottom of the conduction band and/or top of the valence band increases with decreasing thickness of the electron pocket. This phenomenon is the well-known quantum size effect, which has been widely applied in optoelectronic devices such as light emitting diodes and laser diodes based on GaAs (Refs. 1 and 2) and GaN.[3]

Utilization of the quantum size effect should also be beneficial in obtaining high performance thermoelectric materials. In 1993, Hicks and Dresselhaus[4] theoretically predicted that the thermoelectric figure of merit $Z_{2D}T$ ($=S^2\sigma T\kappa^{-1}$, where Z_{2D}, T, S, σ, and κ are figure of merit, absolute temperature, Seebeck coefficient, electrical conductivity, and thermal conductivity, respectively) of thermoelectric semiconductors can be dramatically enhanced by use of superlattices, with electrons confined in the resulting quantum wells, because the only effect is that the S value increases with DOS without other values decreasing. Their prediction was experimentally confirmed in that two dimensionally confined electrons in 1.5-nm-thick electron pockets in a PbTe (1.5 nm)/$Pb_{0.927}Eu_{0.073}Te$ (45 nm) superlattice exhibit large S_{2D} values as compared to the corresponding PbTe bulk ($S_{2D}/S_{bulk}\sim 2$).[5] Thus, the highest $Z_{2D}T$ can be realized if conduction electrons are confined within the narrowest possible two-dimensional (2D) space, i.e., one unit cell layer.

Very recently, we briefly reported that a high density 2D electron gas (2DEG), which was confined within a unit cell layer thickness (0.3905 nm) in $SrTiO_3$, exhibited a giant $|S|_{2D}$, which was about five times larger than that of the bulk $SrTiO_3$, whereas the 2DEG system retained a rather high σ_{2D} value.[6,7] The 2DEG in $SrTiO_3/SrTi_{0.8}Nb_{0.2}O_3$ superlattices may be a promising candidate for the next generation of thermoelectrics because this system has several advantages such as good environmental compatibility and high thermal and chemical stability as compared to conventional thermoelectric semiconductors such as Bi_2Te_3 and PbTe.[8]

For practical thermoelectric application of these superlattices, clarification of the $SrTiO_3$ barrier thickness dependence of the $|S|_{2D}$ value for $SrTiO_3/SrTi_{0.8}Nb_{0.2}O_3$ superlattices is critically important because insulating $SrTiO_3$ barrier thickness must be minimized to improve effective $Z_{3D}T$. Here, we report the details of the giant $|S|_{2D}$ of the $SrTiO_3/SrTi_{0.8}Nb_{0.2}O_3$ superlattices. We measured $|S|_{2D}$ values of $[(SrTiO_3)_x/(SrTi_{0.8}Nb_{0.2}O_3)_y]_{20}$ ($x=1-60$, $y=1-20$) superlattices. The $|S|_{2D}$ value increased proportionally to $y^{-0.5}$ and reached 320 $\mu V\ K^{-1}$ ($x=17$, $y=1$), which is approximately five times larger than that of the $SrTi_{0.8}Nb_{0.2}O_3$ bulk ($|S|_{3D}=61\ \mu V\ K^{-1}$). This is clear evidence that the origin of the giant $|S|_{2D}$ is 2D quantum confinement of conduction electrons in the $SrTi_{0.8}Nb_{0.2}O_3$ layer. Further, we also clarified that the critical barrier $SrTiO_3$ thickness for quantum confinement of conduction electrons is 6.25 nm (16 unit cells of $SrTiO_3$).

Superlattices of $[(SrTiO_3)_x/(SrTi_{0.8}Nb_{0.2}O_3)_y]_z$ ($x=0-60$, $y=1-20$, $z=20$) were fabricated on the (001) face of $LaAlO_3$ substrates[9] by pulsed laser deposition (KrF excimer laser, $\lambda=248$ nm, 20 ns, 10 Hz, and $\sim 1\ J\ cm^{-2}\ pulse^{-1}$) at 950 °C in an oxygen atmosphere (oxygen pressure $PO_2=1\times10^{-3}$ Pa). A $SrTiO_3$ single crystal plate and a $SrTi_{0.8}Nb_{0.2}O_3$ ceramic were used as targets. During film growth of the superlattices, the intensity oscillation of reflection high-energy electron diffraction (RHEED) spots [Fig. 1(a) inset] was monitored to count the number of

[a]Author to whom correspondence should be addressed. Electronic mail: h-ohta@apchem.nagoya-u.ac.jp

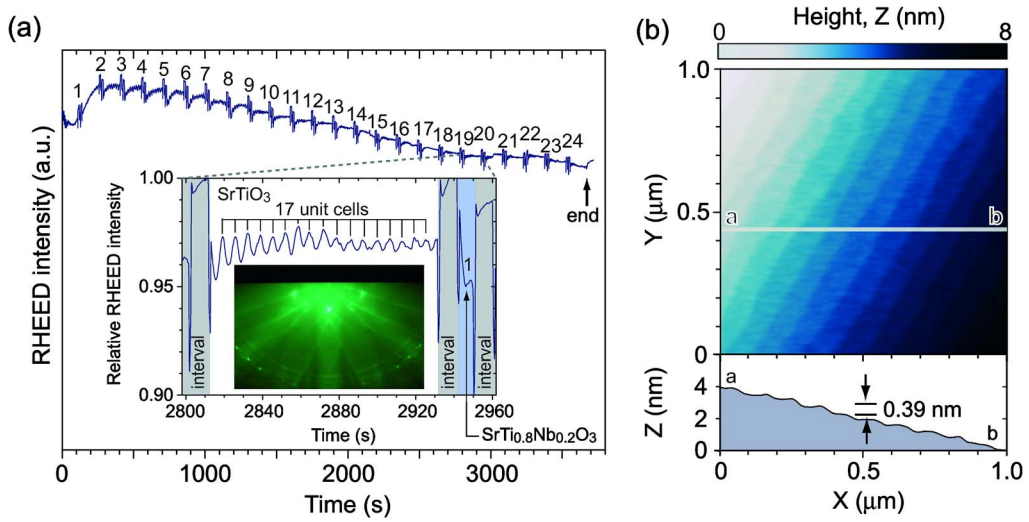

FIG. 1. (Color online) (a) RHEED intensity oscillation during the film growth of the $[(SrTiO_3)_{17}/(SrTi_{0.8}Nb_{0.2}O_3)_1]_{24}$ superlattice. (b) Topographic AFM image of the superlattice film of $[(SrTiO_3)_{17}/(SrTi_{0.8}Nb_{0.2}O_3)_1]_{24}$. Atomically flat terraced and stepped structures are seen.

$SrTiO_3$ or $SrTi_{0.8}Nb_{0.2}O_3$ layers. Figure 1(a) shows the typical RHEED oscillation pattern during the growth of $[(SrTiO_3)_{17}/(SrTi_{0.8}Nb_{0.2}O_3)_1]_{24}$. The inset shows the magnified oscillation pattern. RHEED intensity oscillations were observed throughout the growth of the superlattices. Atomically flat terraces and steps, which correspond to a unit cell height of $SrTiO_3$, are clearly seen in the atomic force microscopic (AFM) (Nanoscope E, Digital Instruments) image [Fig. 1(b)], indicating that 2D growth occurred.

Satellite peaks due to superlattices are clearly observed in the x-ray diffraction (XRD) (ATX-G, Rigaku Co.) patterns of $[(SrTiO_3)_{17}/(SrTi_{0.8}Nb_{0.2}O_3)_y]_z$ ($y=1$, 2, 4, 8, and 16) [Fig. 2(a)] around the Bragg peak of 002 $SrTiO_3$ (0). Further, the period of the superlattices, which was calculated from the XRD patterns, corresponds well with those desired [Fig. 2(a) inset]. Figure 2(b) shows a Cs-corrected high-angle angular dark-field scanning transmission electron microscope (HAADF-STEM) (JEOL-2100F)[10] image of the $[(SrTiO_3)_{24}/(SrTi_{0.8}Nb_{0.2}O_3)_1]_{20}$ superlattice and a Ti–$L_{2,3}$ edge electron energy loss spectral (EELS) profile. Stripe-shaped contrast is clearly seen in the HAADF-STEM image. Further, the image intensity at the Ti column in one unit cell thickness of $SrTi_{0.8}Nb_{0.2}O_3$ shows higher intensity than that of the $SrTiO_3$ barrier layer, and the Ti–$L_{2,3}$ edge EELS from the Nb-doped layer shows broad profiles in the arrowed region,[11] confirming that the doped Nb^{5+} ions and electrons are exclusively confined in the $SrTi_{0.8}Nb_{0.2}O_3$ layer. From these results, we conclude that high-quality $[(SrTiO_3)_{17}/(SrTi_{0.8}Nb_{0.2}O_3)_y]_z$ superlattices were successfully fabricated.

We then measured the carrier concentrations (n_e) and Hall mobilities (μ_{Hall}) of the superlattices at room temperature (300 K); for the $SrTi_{0.8}Nb_{0.2}O_3$ film, these were 4.3×10^{21} cm^{-3} and 5 $cm^2\ V^{-1}\ s^{-1}$, respectively, while values of the undoped $SrTiO_3$ film were impossible to measure because of its low n_e ($\ll10^{15}$ cm^{-3}). The observed n_e and μ_{Hall} values of the superlattices are summarized in Table I. Since the n_e value of the $SrTiO_3$ barrier layer is very low ($\ll10^{15}$ cm^{-3}), the n_e value of the $SrTi_{0.8}Nb_{0.2}O_3$ layer of $[(SrTiO_3)_x/(SrTi_{0.8}Nb_{0.2}O_3)_y]_z$ is estimated to be $n_{e\text{obs}}(x+y)/y$ ($\sim4\times10^{21}$ cm^{-3}), agreeing well with that of the $SrTi_{0.8}Nb_{0.2}O_3$ film. Generally, the $|S|$ value of a multilayered film is given by $\Sigma|S|_i\sigma_{xxi}/\Sigma\sigma_{xxi}$,[12] where $|S|_i$ and σ_{xxi} are the Seebeck coefficient and sheet conductivity of the ith layer, respectively. In the present case, we directly measured S_{2D} of the $SrTi_{0.8}Nb_{0.2}O_3$ layer, since σ_{xxi} of the $SrTi_{0.8}Nb_{0.2}O_3$ layer is at least six orders of magnitude larger than that of the $SrTiO_3$ barrier layer.

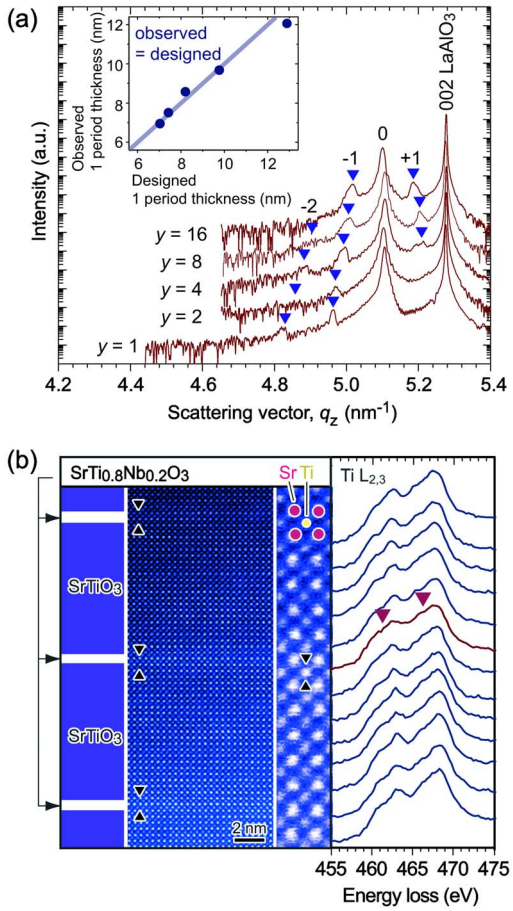

FIG. 2. (Color online) (a) Out-of-plane XRD patterns of $[(SrTiO_3)_{17}/(SrTi_{0.8}Nb_{0.2}O_3)_y]_z$ superlattices ($y=1$, 2, 4, 8, and 16). Intense Bragg peak of the superlattices are seen together with the −2nd, −1st and +1st satellites. The period of the superlattices corresponds well with that desired (inset). (b) HAADF-STEM image and Ti–$L_{2,3}$ edge EELS profile. The image intensity at the Ti column in a one unit cell thickness of $SrTi_{0.8}Nb_{0.2}O_3$ shows higher intensity than that of the $SrTiO_3$ barrier layer, and the Ti–$L_{2,3}$ edge EELS from the Nb-doped layer shows a broad profile in the arrowed region, confirming that the doped Nb^{5+} ions and electrons are exclusively confined in the $SrTi_{0.8}Nb_{0.2}O_3$ layer.

TABLE I. Observed n_e and μ_{Hall} values of the $[(SrTiO_3)_{17}/(SrTi_{0.8}Nb_{0.2}O_3)_y]_{20}$ superlattices at room temperature. The n_e values of the $SrTi_{0.8}Nb_{0.2}O_3$ layer in $[(SrTiO_3)_x/(SrTi_{0.8}Nb_{0.2}O_3)_y]_{20}$ are estimated as $n_{e\mathrm{obs}}(x+y)/y$.

y	Observed n_e (10^{21} cm^{-3})	$n_{e:\mathrm{Nb\text{-}doped}}$ (10^{21} cm^{-3})	μ_{Hall} (cm^2 V^{-1} s^{-1})
1	0.22	4.0	6.3
2	0.27	3.0	6.8
4	0.66	3.1	5.6
8	1.1	3.4	5.1
16	2.0	4.2	5.3

The $|S|_{2D}$ values of the $[(SrTiO_3)_x/(SrTi_{0.8}Nb_{0.2}O_3)_y]_z$ superlattices were measured at room temperature by a conventional steady state method, introducing a temperature gradient in the in-plane direction. Figure 3(a) shows $|S|_{2D}$-y plots for $[(SrTiO_3)_x/(SrTi_{0.8}Nb_{0.2}O_3)_y]_z$ superlattices. A dramatic increase of $|S|_{2D}$ is seen with decreasing y-value. When y is 1, $|S|_{2D}$ reaches 320 μV K^{-1}, which is approximately times larger than that of the $SrTi_{0.8}Nb_{0.2}O_3$ bulk ($|S|_{3D}$=61 μV K^{-1}). The slope of the plot of log$|S|_{2D}$ versus log y is −0.5, as shown in the inset, most likely suggesting DOS(E)$\propto y^{-1.0}$, where E is the ground state energy, which for the quantum well is given by $E=(h^2/2m_d^\star)(\pi/L_z)^2$,[13] where

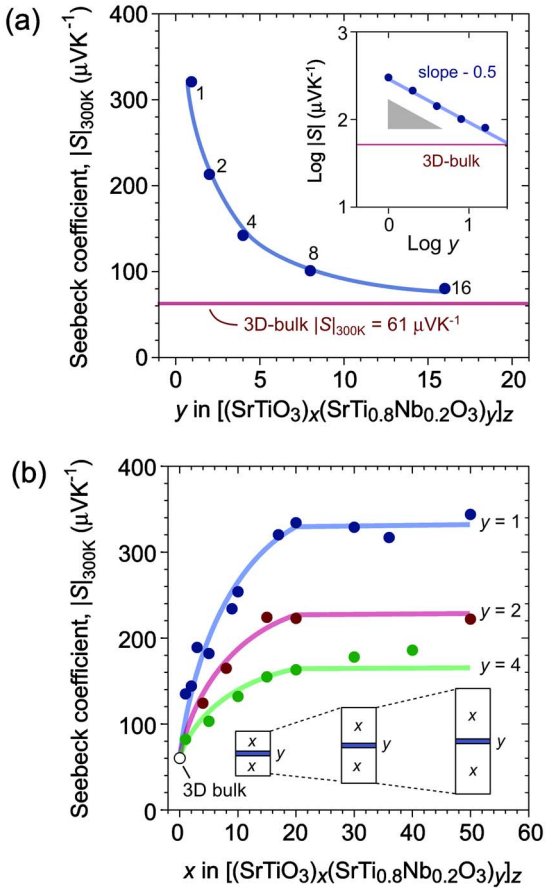

FIG. 3. (Color online) (a) $|S|_{2D}$-y plots for the $[(SrTiO_3)_x/(SrTi_{0.8}Nb_{0.2}O_3)_y]_z$ superlattices. A dramatic increase of $|S|_{2D}$ is seen with decreasing y. Plots of log$|S|_{2D}$-log y are shown in the inset. (b) $|S|_{2D}$-x plots for $[(SrTiO_3)_x/(SrTi_{0.8}Nb_{0.2}O_3)_y]_z$ (y=1, 2, and 4) superlattices. Saturation of the $|S|_{2D}$ value is seen when $x>16$ (6.25 nm) in all cases.

h, $m_d^\star$, and L_z are the Planck constant, DOS effective mass, and width of the quantum well, respectively. Since the $m_d^\star$ value of $SrTiO_3$ is $7m_0$,[14–16] we obtained E values of 352 and 1.4 meV using L_z values of 0.3905 nm (y=1) and 6.248 nm (y=16), respectively. DOS(E) at the ground state for y=1, which is given by $(1/2\pi^2)(2m_d^\star/h^2)^{3/2}\sqrt{E}$, is estimated to be 7.5×10^{22} cm^{-3} eV^{-1}, 16 times larger than that for y=16 (4.7×10^{21} cm^{-3} eV^{-1}). We conclude that the dramatic increase in DOS(E) at the ground state is the origin of the giant Seebeck coefficient.

Figure 3(b) shows $|S|_{2D}$-x plots for $[(SrTiO_3)_x/(SrTi_{0.8}Nb_{0.2}O_3)_y]_z$ (y=1, 2, and 4) superlattices. The $|S|_{2D}$ value increases monotonically with x and saturates when $x>16$ (6.25 nm) in all cases. Thus, we have successfully clarified that the critical barrier thickness for electron tunneling in the $[(SrTiO_3)_x/(SrTi_{0.8}Nb_{0.2}O_3)_y]_z$ superlattice is 6.25 nm (16 unit cell layers of $SrTiO_3$).

In summary, we have clarified the origin of the giant 2D-Seebeck coefficient ($|S|_{2D}$) of $[(SrTiO_3)_x/(SrTi_{0.8}Nb_{0.2}O_3)_y]_z$ superlattices. A dramatic increase in $|S|_{2D}$ was observed with decreasing y value. When y was 1, $|S|_{2D}$ reaches 320 μV K^{-1}, which is approximately five times larger than that of the $SrTi_{0.8}Nb_{0.2}O_3$ bulk ($|S|_{3D}$ =61 μV K^{-1}). The slope of the log$|S|_{2D}$-log y plot was −0.5, proving that the density of states at the ground state for $SrTiO_3$ increases inversely proportionally to y. The critical barrier thickness for quantum electron confinement was also clarified to be 6.25 nm (16 unit cells of $SrTiO_3$).

This work was financially supported by the Industrial Technology Research Grant Program in 2005 from the New Energy and Industrial Technology Development Organization (NEDO), and a Grant-in-Aid for Scientific Research from the Ministry of Education, Culture, Sports, Science and Technology (No. 18686054).

[1] L. L. Chang, L. Esaki, and R. Tsu, Appl. Phys. Lett. **24**, 593 (1974).
[2] L. Esaki and L. L. Chang, Phys. Rev. Lett. **33**, 495 (1974).
[3] T. Takeuchi, S. Sota, M. Katsuragawa, M. Komori, H. Takeuchi, H. Amano, and I. Akasaki, Jpn. J. Appl. Phys., Part 2 **36**, L382 (1997).
[4] L. D. Hicks and M. S. Dresselhaus, Phys. Rev. B **47**, 12727 (1993).
[5] L. D. Hicks, T. C. Harman, X. Sun, and M. S. Dresselhaus, Phys. Rev. B **53**, R10493 (1996).
[6] H. Ohta, S.-W. Kim, Y. Mune, T. Mizoguchi, K. Nomura, S. Ohta, T. Nomura, Y. Nakanishi, M. Hirano, H. Hosono, and K. Koumoto, Nat. Mater. **6**, 129 (2007).
[7] H. Ohta, Y. Mune, K. Koumoto, T. Mizoguchi, and Y. Ikuhara, Thin Solid Films (to be published).
[8] J. Wood, Mater. Today **10**, 15 (2007).
[9] T. Ohnishi, K. Takahashi, M. Nakagawa, M. Kawasaki, M. Yoshimoto, and H. Koinuma, Appl. Phys. Lett. **74**, 2531 (1999).
[10] J. P. Buban, K. Matsunaga, J. Chen, N. Shibata, W. Y. Ching, T. Yamamoto, and Y. Ikuhara, Science **311**, 212 (2006).
[11] A. Ohtomo, D. A. Muller, J. L. Grazul, and H. Y. Hwang, Nature (London) **419**, 378 (2002).
[12] T. Koga, S. B. Cronin, M. S. Dresselhaus, J. L. Liu, and K. L. Wang, Appl. Phys. Lett. **77**, 1490 (2000).
[13] *Frontiers in Materials Technologies*, edited by M. A. Meyers and O. T. Inal (Elsevier, Amsterdam, 1985), 478.
[14] H. P. R. Frederikse, W. R. Thurber, and W. R. Hosler, Phys. Rev. **134**, A442 (1964).
[15] S. Ohta, T. Nomura, H. Ohta, M. Hirano, H. Hosono, and K. Koumoto, Appl. Phys. Lett. **87**, 092108 (2005).
[16] M. Yamamoto, H. Ohta, and K. Koumoto, Appl. Phys. Lett. **90**, 072101 (2007).